Constraining Exoplanet Mass from Transmission Spectroscopy

Julien de Wit and Sara Seager

Science **342**, 1473 (2013);
DOI: 10.1126/science.1245450

28. K. Wakamatsu, M. Fujimoto, M. Nakazono, S. Arimura, N. Tsutsumi, *Plant Cell Rep.* **29**, 1139–1145 (2010).
29. P.-A. Christin *et al.*, *Curr. Biol.* **22**, 445–449 (2012).
30. D. L. Nickrent, V. Malécot, R. Vidal-Russell, J. P. Der, *Taxon* **59**, 538–558 (2010).
31. P. Morat *et al.*, *Adansonia sér. 3* **34**, 177–219 (2012).
32. W. F. Doolittle, *Proc. Natl. Acad. Sci. U.S.A.* **110**, 5294–5300 (2013).

Acknowledgments: We thank E. Dalin, J. Gummow, and P. Lowry for assistance; R. Wing and the Arizona Genomics Institute for *Amborella* bacterial artificial chromosome sequences; the North and South Environmental Services of New Caledonia for collecting permits; M. Moore, P. Soltis, and D. Soltis for two unpublished plastid-genome sequences; and those individuals (see table S11) who supplied the photographs for figures. This work was supported by NIH-RO1-GM-76012 (J.D.P. and E.B.K), the U.S. Department of Energy–Joint Genome Institute Community Sequencing Program under contract DE-AC02-05CH11231 (J.D.P, E.B.K, and J.L.B), NSF-GRF-112955 (A.O.R.), NSF-DBI-0638595 (C.W.D), and the METACyt Initiative of Indiana University, funded by the Lilly Endowment. The data reported in this paper are deposited in GenBank under accessions KF754799-KF754803 and KF798319-KF798355.

Supplementary Materials
www.sciencemag.org/content/342/6165/1468/suppl/DC1
Materials and Methods
Figs. S1 to S23
Tables S1 to S12
References (*33*–*76*)

23 September 2013; accepted 11 November 2013
10.1126/science.1246275

Constraining Exoplanet Mass from Transmission Spectroscopy

Julien de Wit[1]* and Sara Seager[1,2]

Determination of an exoplanet's mass is a key to understanding its basic properties, including its potential for supporting life. To date, mass constraints for exoplanets are predominantly based on radial velocity (RV) measurements, which are not suited for planets with low masses, large semimajor axes, or those orbiting faint or active stars. Here, we present a method to extract an exoplanet's mass solely from its transmission spectrum. We find good agreement between the mass retrieved for the hot Jupiter HD 189733b from transmission spectroscopy with that from RV measurements. Our method will be able to retrieve the masses of Earth-sized and super-Earth planets using data from future space telescopes that were initially designed for atmospheric characterization.

With more than 900 confirmed exoplanets (*1*) and more than 2300 planetary candidates known (*2*), research priorities are moving from planet detection to planet characterization. In this context, a planet's mass is a fundamental parameter because it is connected to a planet's internal and atmospheric structure and it affects basic planetary processes, such as the cooling of a planet, its plate tectonics (*3*), magnetic field generation, outgassing, and atmospheric escape. Measurement of a planetary mass can in many cases reveal the planet bulk composition, allowing us to determine whether the planet is a gas giant or is rocky and suitable for life as we know it.

Planetary mass is traditionally constrained with the radial velocity (RV) technique using single-purpose dedicated instruments. The RV technique measures the Doppler shift of the stellar spectrum to derive the planet-to-star (minimum) mass ratio as the star orbits the planet-star common center of mass. Although the RV technique has a pioneering history of success laying the foundation of the field of exoplanet detection, it is mainly effective for massive planets around relatively bright and quiet stars. Most transiting planets have host stars that are too faint for precise RV measurements. For sufficiently bright host stars, stellar perturbations may be larger than the planet's signal, preventing a determination of the planet mass with RV measurements even for hot Jupiters (*4*). In the long term, the limitation due to the faintness of targets will be reduced with technological improvements. However, host-star perturbations may be a fundamental limit that cannot be overcome, meaning that the masses of small planets orbiting quiet stars would remain out of reach. Current alternative mass measurements to RV for transiting planets are based on modulations of planetary-system light curves (*5*) or transit-timing variations (*6*). The former works for massive planets on short period orbits and involves detection of both beaming and ellipsoidal modulations (*7*). The latter relies on gravitational perturbations of a companion on the transiting planet's orbit. This method is most successful for companions that are themselves transiting and in orbital resonance with the planet of interest (*8*, *9*). For unseen companions, the mass of the transiting planet is not constrained, but an upper limit on the mass of the unseen companion can be obtained to within 15 to 50% (*10*).

Transiting exoplanets are of special interest because the size of a transiting exoplanet can be derived from its transit light curve and combined with its mass, if known, to yield the planet's

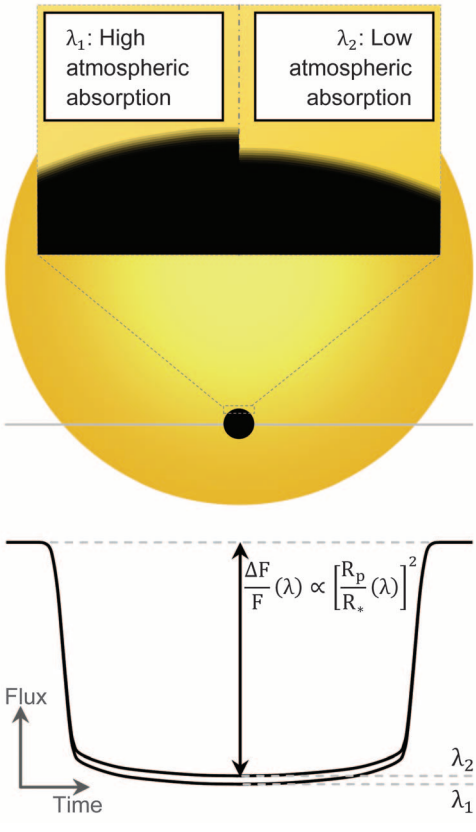

Fig. 1. Transit-depth variations, $\frac{\Delta F}{F}(\lambda)$, induced by the wavelength-dependent opacity of a transiting planet atmosphere. The stellar disk and the planet are not resolved; the flux variation of a point source is observed.

[1]Department of Earth, Atmospheric and Planetary Sciences, Massachusetts Institute of Technology, 77 Massachusetts Avenue, Cambridge, MA 02139, USA. [2]Department of Physics, Massachusetts Institute of Technology, 77 Massachusetts Avenue, Cambridge, MA 02139, USA.

*Corresponding author. E-mail: jdewit@mit.edu

density, constraining its internal structure and potential habitability. Furthermore, the atmospheric properties of a transiting exoplanet can be retrieved from the host-star light passing through its atmosphere when it transits, but the quality of atmospheric retrieval is reduced if the planet's mass is inadequately constrained (*11*).

Here, we introduce MassSpec, a method for constraining the mass of transiting exoplanets based solely on transit observations. MassSpec extracts a planet's mass through its influence on the atmospheric scale height. It simultaneously and self-consistently constrains the mass and the atmosphere of an exoplanet, provides independent mass constraints for transiting planets accessible to RV, and allows us to determine the masses of transiting planets for which the RV method fails.

MassSpec: Concept and Feasibility

The mass of a planet affects its transmission spectrum through the pressure profile of its atmosphere [i.e., $p(z)$, where z is the altitude], and hence its atmospheric absorption profile. For an ideal gas atmosphere in hydrostatic equilibrium, the pressure varies with the altitude as $d\ln(p) = -\frac{1}{H}dz$, where H is the atmospheric scale height defined as

$$H = \frac{kT}{\mu g} \quad (1)$$

where k is Boltzmann's constant and T, μ, and g are the local (i.e., altitude dependent) temperature, mean molecular mass, and gravity. By expressing the local gravity in terms of the planet's mass (M_p) and radius (R_p), Eq. 1 can be rewritten as

$$M_p = \frac{kTR_p^2}{\mu GH} \quad (2)$$

Thus, our method conceptually requires constraining the radius of the target as well as its atmospheric temperature, mean molecular mass, and scale height.

A planet transmission spectrum can be seen as a wavelength-dependent drop in the apparent brightness of the host star when the planet transits (Fig. 1). At a wavelength with high atmospheric absorption, λ_1, the planet appears larger than at a wavelength with lower atmospheric absorption, λ_2, because of the additional flux drop due to the opaque atmospheric annulus. In particular, a relative flux drop, $\frac{\Delta F}{F}(\lambda)$, is associated with an apparent planet radius, $R_p(\lambda) = \sqrt{\frac{\Delta F}{F}(\lambda)} \times R_*$. Transmission spectroscopy mainly probes low-pressure levels; therefore, the mass encompassed in the sphere of radius $R_p(\lambda)$ (Eq. 2) is a good proxy for the planetary mass. The apparent radius of a planet relates directly to its atmospheric properties due to their effect on its opacity

$$\pi R_p^2(\lambda) = \pi[R_{p,0} + h_{eff}(\lambda)]^2 = \int_0^\infty 2\pi r(1 - e^{-\tau(r,\lambda)})dr \quad (3)$$

where $R_{p,0}$, $h_{eff}(\lambda)$, and $e^{-\tau(r,\lambda)}$ are, respectively, a planetary radius of reference—i.e., any radial distance at which the body is optically thick in limb-looking over all the spectral band of interest, the effective atmosphere height, and the planet's transmittance at radius r (Fig. 2). $\tau(r,\lambda)$ is the slant-path optical depth defined as

$$\tau(r,\lambda) = 2\int_0^{x_\infty} \sum_i n_i(r') \times \sigma_i[T(r'),p(r'),\lambda]dx \quad (4)$$

where $r' = \sqrt{r^2 + x^2}$ and $n_i(r')$ and $\sigma_i[T(r'),p(r'),\lambda]$ are the number density and the extinction cross section of the ith atmospheric component at the radial distance r′ (*12*). In other words, a planet's atmospheric properties [$n_i(z)$, $T(z)$, and $p(z)$] are embedded in its transmission spectrum through $\tau(r,\lambda)$ (Eqs. 3 and 4). The integral in Eq. 3 can be split at the radius of reference (because the planet is opaque at all λ at smaller radii), and thus Eq. 3 becomes

$$[R_{p,0} + h_{eff}(\lambda)]^2 = R_{p,0}^2 + c \quad (5)$$
$$c \triangleq 2\int_0^{z_\infty} (R_{p,0} + z)(1 - e^{-\tau(z,\lambda)})dz$$

leading directly to the expression of the effective atmosphere height

$$h_{eff}(\lambda) = R_{p,0}(-1 + \sqrt{1 + c}) \quad (6)$$

The embedded atmospheric information can be straightforwardly accessed for most optically active wavelength ranges using

$$h_{eff}(\lambda) = R_{p,0}B(\gamma_{EM} + \ln A_\lambda) \quad (7)$$

where γ_{EM} is the Euler-Mascheroni constant (*13*): $\gamma_{EM} = \lim_{n\to+\infty}\sum_{k=1}^{n}\frac{1}{k} - \ln n \approx 0.57722$ (supplementary text 1) (*14*). In the above equation, B is a multiple of the dimensionless scale height and A_λ is an extended slant-path optical depth at the reference radius. The exact formulation of B and A_λ depends on the extinction processes affecting the transmission spectrum at λ (table S1). For Rayleigh scattering

$$B = \frac{H}{R_{p,0}} \text{ and} \quad (8)$$

$$A_\lambda = \sqrt{2\pi R_{p,0}H}n_{sc,0}\sigma_{sc}(\lambda) \quad (9)$$

where $n_{sc,0}$ and $\sigma_{sc}(\lambda)$ are the number density at $R_{p,0}$ and the cross-section of the scatterers. Conceptually, Eq. 7 tells us the altitude where the atmosphere becomes transparent for a given slant-path optical depth at a radius of reference, A_λ. For example, if A_λ is 10^4, then the atmosphere becomes transparent at ≈ 9 scale heights above the reference radius.

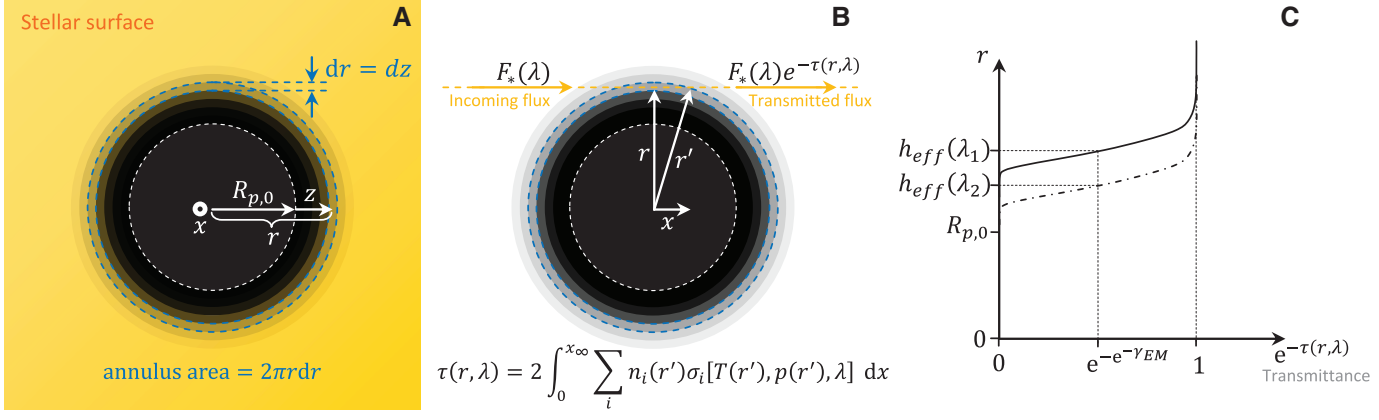

Fig. 2. Basics of a planet's transmission spectrum (planetary atmosphere scaled up to enhance visibility). (**A**) In-transit geometry as viewed by an observer presenting the areas of the atmospheric annulii affecting the transmission spectrum. (**B**) Side view showing the flux transmitted through an atmospheric annulus of radius r. (**C**) Transmittance as a function of the radius at wavelengths with high and low atmospheric absorption: λ_1 (solid lines) and λ_2 (dash-dotted lines), respectively. Due to higher atmospheric absorption at λ_1, the planet will appear larger than it does at λ_2 because of the more-extended opaque atmospheric annulus [$h_{eff}(\lambda_1) > h_{eff}(\lambda_2)$] that translates into an additional flux drop (*14*).

Most important, Eq. 7 reveals the dependency of a transmission spectrum on its key parameters: In particular, A_λ is dependent in unique ways on the scale height, the reference pressure, the temperature, and the number densities of the main atmospheric absorbents (supplementary text 1.4), which lead to the mean molecular mass. The uniqueness of these dependencies enables the independent retrieval of each of these key parameters. Therefore, a planet's mass can be constrained uniquely by transmission spectroscopy (Eq. 2).

MassSpec: Applications

Gas Giants

With available instruments, MassSpec is applicable only to hot Jupiters. Their mean molecular mass is known a priori (H/He-dominated atmosphere: $\mu \approx 2.3$), and their temperature is inferred from, for example, emission spectroscopy. Hence, high signal-to-noise ratio (SNR)/resolution transmission spectra are not required to constrain their mean molecular mass and temperature independently. Therefore, the measurement of the Rayleigh-scattering slope in transmission is sufficient to yield the mass of a hot Jupiter because it relates directly to its atmospheric scale height. Because A_λ depends solely on λ through $\sigma_{sc}(\lambda)$ for Rayleigh scattering (Eq. 9), using the scaling law function for the Rayleigh-scattering cross section, $\sigma_{sc}(\lambda) = \sigma_0(\lambda/\lambda_0)^\alpha$, Eq. 7 leads to

$$\alpha H = \frac{dR_p(\lambda)}{d\ln\lambda} \quad (10)$$

with $\alpha = -4$ (*15*). Therefore, using Eqs. 2 and 10, the planet mass can be derived from

$$M_p = -\frac{4kT[R_p(\lambda)]^2}{\mu G \frac{dR_p(\lambda)}{d\ln\lambda}} \quad (11)$$

Based on estimates (*16*, *17*) of $T \approx 1300$ K, $dR_p(\sim 0.8\ \mu m)/d\ln\lambda \approx -920$ km, and $R_p(\sim 0.8\ \mu m) \approx 1.21\ R_{Jup}$ derived from emission and transmission spectra, MassSpec's estimate of HD 189733b's mass is 1.15 M_{Jup}. This is in excellent agreement with the mass derived from RV measurements [$1.14 \pm 0.056\ M_{Jup}$ (*18*)] for this extensively observed Jovian exoplanet. MassSpec's application to gas giants will be particularly important for gas giants whose star's activity prevents a mass measurement with RV [e.g., the hottest known planet, WASP-33b (*4*)].

Super-Earths and Earth-Sized Planets

The pool of planets accessible to MassSpec will extend down to super-Earths and Earth-sized planets thanks to the high SNR spectra expected from the James Webb Space Telescope (JWST) (launch date 2018) and the Exoplanet Characterisation Observatory (EChO) (European Space Agency M3 mission candidate). We estimate that with data from JWST, MassSpec could yield the mass of mini-Neptunes, super-Earths, and Earth-sized planets up to distances of 500 pc, 100 pc, and 50 pc, respectively, for M9V stars and 200 pc, 40 pc, and 20 pc for M1V stars or stars with earlier spectral types (Fig. 3 and supplementary text 2.4). For EChO, the numbers would be 250 pc, 50 pc, and 13 pc, and 100 pc, 20 pc, and 6 pc, respectively.

In particular, if MassSpec were applied to 200 hours of in-transit observations of super-Earths transiting an M1V star at 15 pc with JWST, it would yield mass measurements with a relative uncertainty of ~2%, ~10%, and ~15% for hydrogen-, water-, or nitrogen-dominated atmospheres, respectively (Fig. 4 and figs. S9 and S10). The larger significance of the mass measurements obtained for hydrogen-dominated super-Earths results from higher SNR of their transmission spectra, which is due to the larger extent of the atmosphere because of the smaller mean molecular mass of H/He. For the same super-Earths with hydrogen- or water-dominated atmospheres, EChO's data should yield mass measurements with a relative uncertainty of ~3% or ~25% (figs. S11 and S12), respectively; for a nitrogen world in the same configuration, it will not be possible to constrain the mass (fig. S13).

In the future era of 20-m space telescopes, sufficiently high-quality transmission spectra of Earth-sized planets will be available (*19*). By using MassSpec, such facilities could yield the mass of Earth-sized planets transiting an M1V star (or stars with earlier spectral types) at 15 pc with a relative uncertainty of ~5% (fig. S17). For M9V stars, it would be possible to constrain the mass of Earth-sized planets up to 200 pc, and for M1V stars or stars with earlier spectral types, up to 80 pc (Fig. 3).

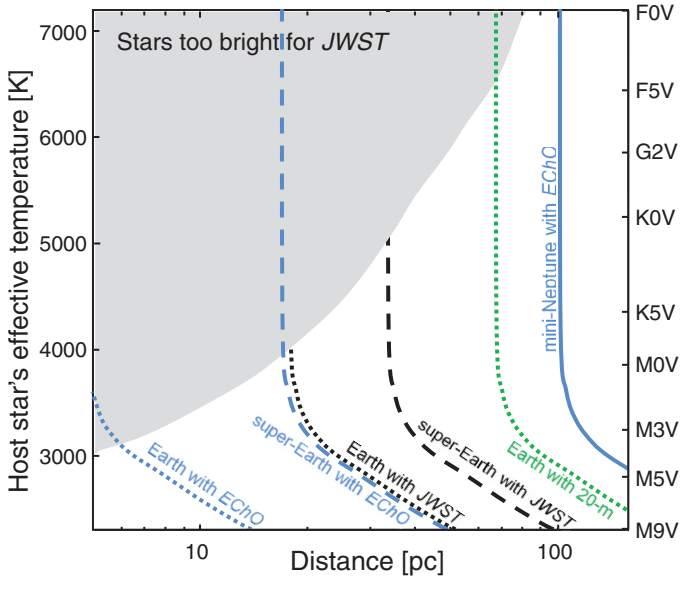

Fig. 3. The boundaries of MassSpec's application domain for 200 hours of in-transit observations. Using JWST, MassSpec could yield the mass of super-Earth and Earth-sized planets up to the distance shown by the black dashed and dotted lines, respectively. Similarly, the maximum distance to Earth for MassSpec's application based on EChO's observations of a mini-Neptune, a super-Earth, and an Earth-sized planet are shown by the blue solid, dashed, and dotted lines, respectively. The green dotted line refers to the case of an Earth-sized planet observed with a 20-m space telescope. The gray area shows the stars too bright for JWST/NIRSpec in the $R = 1000$ mode (J-band magnitude $\lesssim 7$).

Discussion

Finding Habitable Earth-Sized Planets Around Late M Dwarfs in the Next Decade

Late M dwarfs are favorable for any in-transit information, such as transmission spectra, because of their large ratio of radiance over projected area (fig. S19). For that reason, MassSpec can be applied to late M dwarfs more distant than other stars, for a given planet (Fig. 3). If they exist, Earth-sized planets may be detected around late M dwarfs before JWST's launch by SPECULOOS (Search for Habitable Planets Eclipsing Ultra-Cool Stars), a European Research Council mission that will begin observing the coolest M dwarfs in 2016. Their mass will not be constrained by RV because of the faintness of their host stars. However, MassSpec's application to their JWST spectra will yield both their masses and atmospheric properties (Fig. 5), and hence the assessment of their potential habitability.

JWST-EChO Synergy

Time prioritization of JWST and EChO taking into account their synergy would increase the science delivery of both missions. Because the smaller aperture of EChO would enable it to observe brighter stars (i.e., early-type and close-by stars), EChO's and JWST's time could be respectively prioritized on super-Earths and Earth-sized planets for M9V stars closer than 25 pc and for M1V stars (or stars with earlier spectral type) closer than 10 pc (Fig. 3). Similarly, EChO's and JWST's time could be respectively prioritized on gas giants and super-Earths for M9V stars closer than 125 pc and for M1V stars (or stars with earlier spectral type) closer than 50 pc. EChO would be particularly useful to determine the mass and atmospheric

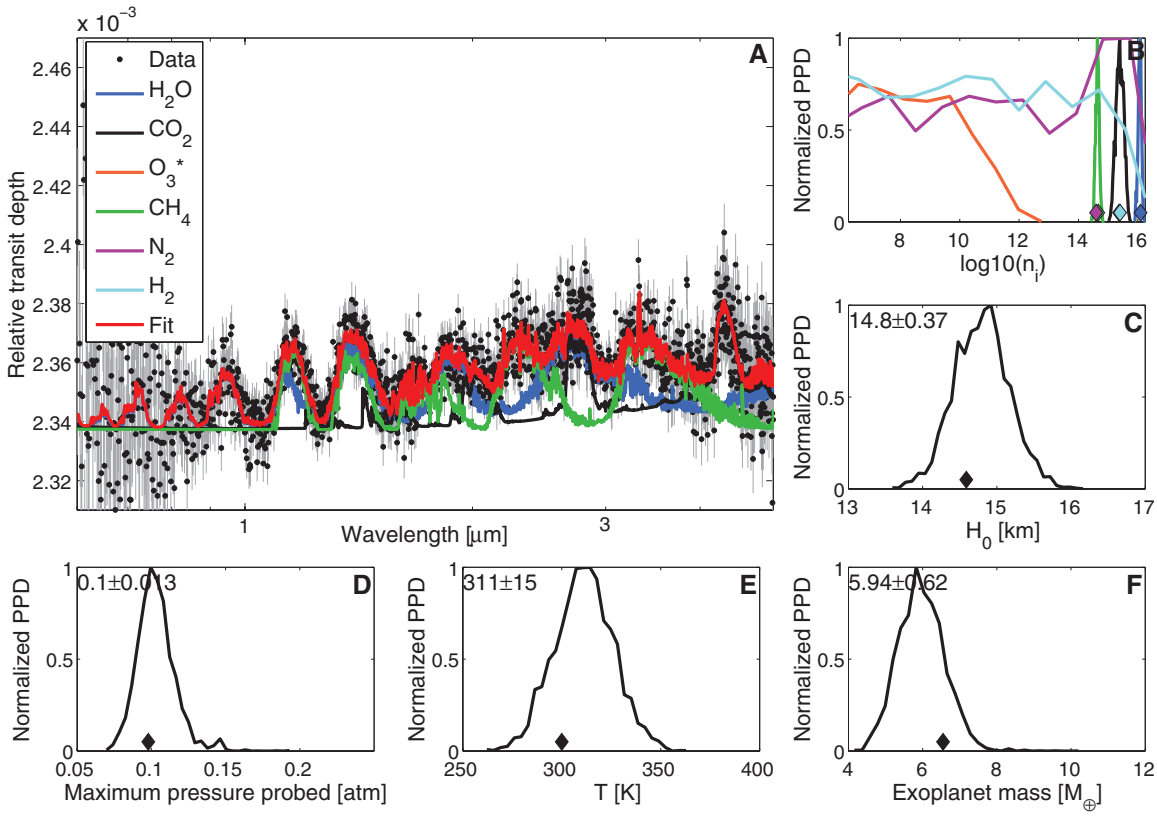

Fig. 4. MassSpec's application to the synthetic transmission spectrum of a water-dominated super-Earth transiting an M1V star at 15 pc as observed with JWST for a total of 200 hours in-transit. (**A**) Synthetic data and the best fit, together with the individual contributions of the atmospheric species. (**B**) Normalized posterior probability distribution (PPD) of the atmospheric species number densities at the reference radius. (**C**) Normalized PPD for the scale height. (**D**) Normalized PPD for the pressure at the deepest atmospheric level probed by transmission spectroscopy. (**E**) Normalized PPD for the temperature. (**F**) Normalized PPD for the exoplanet mass. The diamonds indicate the values of atmospheric parameters used to simulate the input spectrum, and the asterisks in (A) indicate molecules that are not used to simulate the input spectrum. The atmospheric properties (number densities, scale height, and temperature) are retrieved with significance, yielding a mass measurement with a relative uncertainty of ~10%.

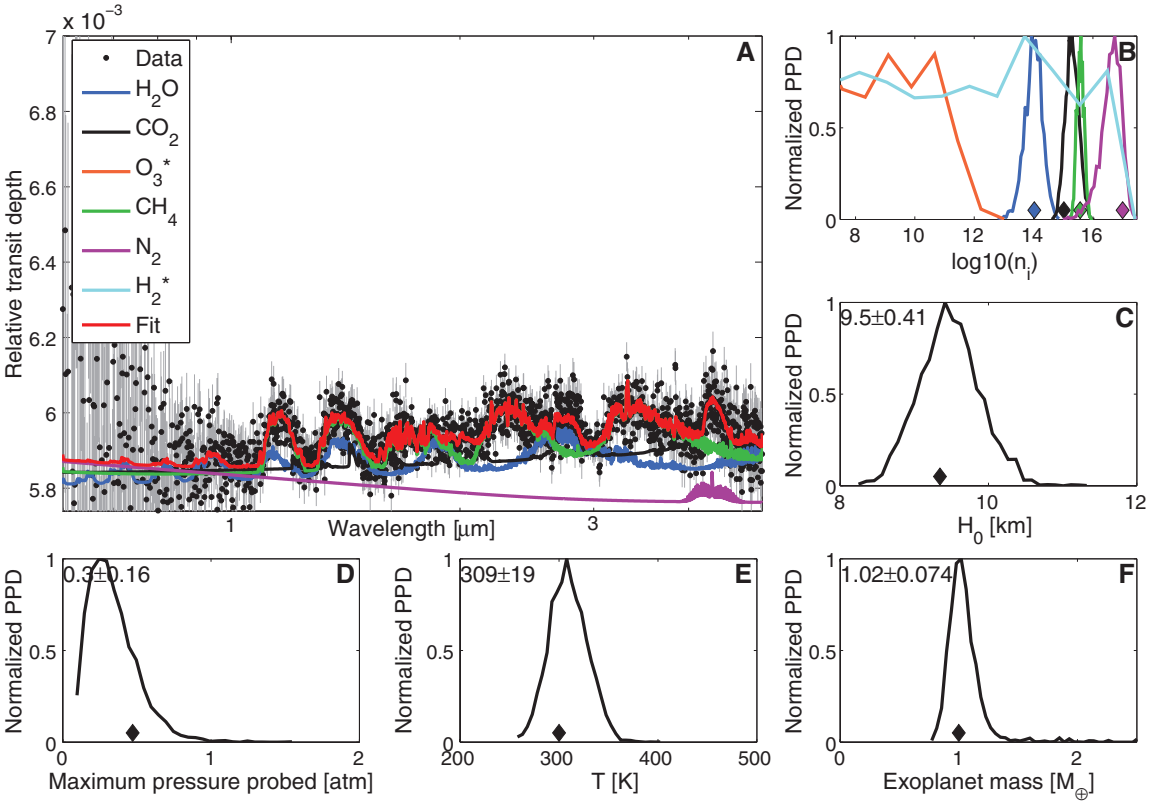

Fig. 5. MassSpec's application to the synthetic transmission spectrum of an Earth-like exoplanet transiting an M7V star at 15 pc as observed with JWST for a total of 200 hours in-transit. (**A** to **F**) show the same quantities as on Fig. 4. The atmospheric properties (number densities, scale height, and temperature) are retrieved with significance, yielding a mass measurement with a relative uncertainty of ~8%.

properties of gas giants because its wide spectral coverage would allow measurement of their Rayleigh-scattering slope at short wavelengths.

Clouds Will Not Overshadow MassSpec

Clouds are known to be present in exoplanet atmospheres (*20*) and to affect transmission spectra by limiting the apparent extent of the molecular absorption bands because the atmospheric layers below the cloud deck are not probed by the observations (*21*). Therefore, the higher the cloud deck, the larger the error bars are with the MassSpec retrieval method due to the reduced amount of atmospheric information available. For example, the uncertainty on the mass estimate of a water-dominated super-Earth with a cloud deck at 1 mbar is twice the uncertainty obtained for the same planet with a cloud-free atmosphere (supplementary text 2.4). However, clouds will not render MassSpec ineffectual because they are not expected for pressures below 1 mbar (*22*), which is at least three orders of magnitude (i.e., seven scale heights) deeper than the lowest pressure probed by transmission spectroscopy. In other words, there will always be atmospheric information available from transmission spectroscopy.

Complementarity of MassSpec and RV

Transmission spectroscopy is suited for low-density planets and atmospheres and bright or large stars (signal $\propto \rho_p^{-1}\mu^{-1}T_*R_*^{0.5}$), whereas radial velocity measurements are ideal for massive planets and low-mass stars (signal $\propto M_p M_*^{-0.5}$). Therefore, each mass-retrieval method is optimal in a specific region of the planet-star parameter space (supplementary text 3), making the methods complementary.

Possible Insights into Planetary Interiors

Mass and radius are not always sufficient to obtain insights into a planet's interior. MassSpec's simultaneous constraints on a planet's atmosphere and bulk density may help to break this degeneracy, in some cases. A precision on a planet mass of 3 to 15%, combined with the planetary radius, can yield the planetary average density and, hence, bulk composition. Even with a relatively low precision of 10 to 15%, it is possible to infer whether a planet is predominantly rocky or predominantly composed of H/He (*23*, *24*). With a higher planet mass precision, large ranges of planetary compositions can be ruled out for high- and low-mass planets, possibly revealing classes of planets with intermediate density to terrestrial-like or ice or giant planets with no solar system counterpart (*25*). Typically, the bulk density alone cannot break the planet interior composition degeneracy, especially for planets of intermediate density. However, measurement of atmospheric species may add enough information to reduce some of the planet interior composition degeneracies—for example, the rejection of H/He as the dominant species yields constraint on the bulk composition, independently of the mass uncertainty.

References and Notes

1. J. Schneider, C. Dedieu, P. Le Sidaner, R. Savalle, I. Zolotukhin, *Astron. Astrophys.* **532**, A79 (2011).
2. N. M. Batalha *et al.*, *Astrophys. J. Supp. Ser.* **204**, 24 (2013).
3. V. Stamenkovic, L. Noack, D. Breuer, T. Spohn, *Astrophys. J.* **748**, 41 (2012).
4. A. C. Cameron *et al.*, *Mon. Not. R. Astron. Soc.* **407**, 507–514 (2010).
5. D. Mislis, R. Heller, J. H. M. M. Schmitt, S. Hodgkin, *Astron. Astrophys.* **538**, A4 (2012).
6. D. C. Fabrycky, *Non-Keplerian Dynamics of Exoplanets* (University of Arizona Press, Tucson, 2010), pp. 217–238.
7. S. Faigler, T. Mazeh, *Mon. Not. R. Astron. Soc.* **415**, 3921–3928 (2011).
8. E. Agol, J. Steffen, R. Sari, W. Clarkson, *Mon. Not. R. Astron. Soc.* **359**, 567–579 (2005).
9. M. J. Holman, N. W. Murray, *Science* **307**, 1288–1291 (2005).
10. J. H. Steffen *et al.*, *Mon. Not. R. Astron. Soc.* **428**, 1077–1087 (2013).
11. J. K. Barstow *et al.*, *Mon. Not. R. Astron. Soc.* **430**, 1188–1207 (2013).
12. S. Seager, *Exoplanet Atmospheres: Physical Processes* (Princeton Univ. Press, Princeton, 2010).
13. L. Euler, *Comm. Acad. Sci. Petropol.* **7**, 150–161 (1740).
14. We also show that Eq. 7 can be rewritten as $\tau[h_{\mathrm{eff}}(\lambda),\lambda] \triangleq \tau_{\mathrm{eq}} = e^{-\gamma_{\mathrm{EM}}}$, meaning that the slant-path optical depth at the apparent height is a constant (Fig. 2C). This extends previous numerical observations that $\tau_{\mathrm{eq}} \approx 0.56$ in some cases (*15*). Therefore, $\tau_{\mathrm{eq}} = \lim_{n\to+\infty} n\prod_{k=1}^{n} e^{-1/k}$ (≈ 0.56146).
15. A. Lecavelier des Etangs, F. Pont, A. Vidal-Madjar, D. Sing, *Astron. Astrophys.* **481**, L83–L86 (2008).
16. N. Madhusudhan, S. Seager, *Astrophys. J.* **707**, 24–39 (2009).
17. F. Pont, H. Knutson, R. L. Gilliland, C. Moutou, D. Charbonneau, *Mon. Not. R. Astron. Soc.* **385**, 109–118 (2008).
18. J. T. Wright *et al.*, *Publ. Astron. Soc. Pac.* **123**, 412–422 (2011).
19. L. Kaltenegger, W. A. Traub, *Astrophys. J.* **698**, 519–527 (2009).
20. B.-O. Demory *et al.*, *Astrophys. J.* **776**, L25 (2013).
21. J. K. Barstow, S. Aigrain, P. G. J. Irwin, L. N. Fletcher, J.-M. Lee, *Mon. Not. R. Astron. Soc.* **434**, 2616–2628 (2013).
22. A. R. Howe, A. S. Burrows, *Astrophys. J.* **756**, 176 (2012).
23. S. Seager, M. Kuchner, C. A. Hier-Majumder, B. Militzer, *Astrophys. J.* **669**, 1279–1297 (2007).
24. J. J. Fortney, M. S. Marley, J. W. Barnes, *Astrophys. J.* **659**, 1661–1672 (2007).
25. L. A. Rogers, P. Bodenheimer, J. J. Lissauer, S. Seager, *Astrophys. J.* **738**, 59 (2011).

Acknowledgments: We are grateful to A. Zsom and V. Stamenkovic for helpful discussions and careful reviews of the manuscript. We also thank S. Messenger, W. Bains, N. Lewis, B.-O. Demory, N. Madhusudhan, A. Triaud, M. Gillon, A. C. Cameron, R. Hu, and B. Benneke. We thank the anonymous referees who helped to improve the paper. J.d.W. thanks G. Cataldo and P. Ferruit for providing information on JWST's Near Infrared Spectrograph (NIRSpec) and A. Belu for further discussions on this matter. J.d.W. acknowledges support from the Wallonie-Bruxelles International, the Belgian American Educational Foundation, and the Grayce B. Kerr Fund in the form of fellowships, as well as from the Belgian Senate in the form of the Odissea Prize. J.d.W. is also particularly grateful to the Duesberg-Baily Thil Lorrain Foundation for its support when he conceived this study.

Supplementary Materials

www.sciencemag.org/content/342/6165/1473/suppl/DC1
Materials and Methods
Supplementary Text
Figs. S1 to S20
Tables S1 and S2
References (*26*–*39*)

2 September 2013; accepted 15 November 2013
10.1126/science.1245450

Crystal Structure of a Soluble Cleaved HIV-1 Envelope Trimer

Jean-Philippe Julien,[1,2,3] Albert Cupo,[4] Devin Sok,[2,3,5] Robyn L. Stanfield,[1,2,3] Dmitry Lyumkis,[1,6] Marc C. Deller,[7] Per-Johan Klasse,[4] Dennis R. Burton,[2,3,5,8] Rogier W. Sanders,[4,9] John P. Moore,[4]* Andrew B. Ward,[1,2,3]* Ian A. Wilson[1,2,3,7,10]*

HIV-1 entry into CD4$^+$ target cells is mediated by cleaved envelope glycoprotein (Env) trimers that have been challenging to characterize structurally. Here, we describe the crystal structure at 4.7 angstroms of a soluble, cleaved Env trimer that is stabilized and antigenically near-native (termed the BG505 SOSIP.664 gp140 trimer) in complex with a potent broadly neutralizing antibody, PGT122. The structure shows a prefusion state of gp41, the interaction between the component gp120 and gp41 subunits, and how a close association between the gp120 V1/V2/V3 loops stabilizes the trimer apex around the threefold axis. The complete epitope of PGT122 on the trimer involves gp120 V1, V3, and several surrounding glycans. This trimer structure advances our understanding of how Env functions and is presented to the immune system, and provides a blueprint for structure-based vaccine design.

The envelope glycoprotein (Env) trimer is the only virally encoded antigen on the surface of HIV-1, the pathogen that causes AIDS, and is responsible for viral entry into host cells. The trimer is composed of gp120/gp41 heterodimers and is the target for neutralizing antibodies. Various structures of components of gp120 and gp41, alone and in complex with different ligands, have been determined (*1*–*10*). Cryogenic electron microscopy (cryo-EM) and tomography have been integrated with core gp120 x-ray structures to visualize the Env trimer at resolutions that extend from 30 Å to below 10 Å and, thereby, provide insights into its overall conformation before and after receptor binding (*11*, *12*). However, determining an atomic-level structure of the Env trimer has been difficult. A higher-resolution structure would not only help to explain how the trimer functions during virus-cell fusion, but also guide HIV-1 vaccine design by delineating the key antigenic sites recognized by the humoral immune system and the defenses evolved by the virus as a countermeasure.